Local Measurements of Viscoelastic Moduli of Entangled Actin Networks Using an Oscillating Magnetic Bead Micro-Rheometer

F. Ziemann, J. Rädler, and E. Sackmann

Department of Physics E22 (Biophysics Group), Technical University of Munich, James-Franck-Strasse, D-85748 Garching, Germany

ABSTRACT   A magnetically driven bead micro-rheometer for local quantitative measurements of the viscoelastic moduli in soft macromolecular networks such as an entangled F-actin solution is described. The viscoelastic response of paramagnetic latex beads to external magnetic forces is analyzed by optical particle tracking and fast image processing. Several modes of operation are possible, including analysis of bead motion after pulse-like or oscillatory excitations, or after application of a constant force. The frequency dependencies of the storage modulus, $G'(\omega)$, and the loss modulus, $G''(\omega)$, were measured for frequencies from 10^{-1} Hz to 5 Hz. For low actin concentrations (mesh sizes $\xi > 0.1$ µm) we found that both $G'(\omega)$ and $G''(\omega)$ scale with $\omega^{1/2}$. This scaling law and the absolute values of G' and G'' agree with conventional rheological measurements, demonstrating that the magnetic bead micro-rheometer allows quantitative measurements of the viscoelastic moduli. Local variations of the viscoelastic moduli (and thus of the network density and mesh size) can be probed in several ways: 1) by measurement of G' and G'' at different sites within the network; 2) by the simultaneous analysis of several embedded beads; and 3) by evaluation of the bead trajectories over macroscopic distances. The latter mode yields absolute values and local fluctuations of the apparent viscosity $\eta(x)$ of the network.

INTRODUCTION

Measurements of the frequency dependence of the viscoelastic moduli provide important insights into the structural and dynamic properties of polymeric fluids and soft macromolecular networks. The latter class includes networks of actin filaments which are prototypes of semi-flexible macromolecules and which may exhibit mesh sizes in the micrometer regime.

Previous studies of the viscoelastic properties of entangled (and cross-linked) F-actin solutions by torsional rheometers (Müller et al., 1991) in the 10^{-5} to 1 Hz regime showed that besides their biological role, these systems are also excellent models of polymeric liquids and can be used to to study fundamental physical properties of such systems, including correlations among the molecular structure, dynamics, and phenomenological properties. The latter is possible since the internal chain dynamics and the reptation motion of actin filaments can be directly visualized and analyzed by dynamic microfluorescence imaging techniques (Käs et al., 1993).

Measurements at high shear rates demonstrate the non-Newtonian behavior of actin networks such as shear thinning (Janmey et al., 1990) and thixotropic effects (Kerst et al., 1990). High precision measurements of the frequency dependencies of the storage ($G'(\omega)$) and loss ($G''(\omega)$) moduli allow studies of the polymerization kinetics of G-actin (Müller et al., 1991) and of subtle effects of actin-binding proteins on filament bending stiffness (Ruddies et al., 1993).

One disadvantage of classical rheological methods is that they yield averages over large volumes, so that effects of local thermal fluctuations and local inhomogenities due to nonequilibrium effects or phase segregation cannot be studied in a straightforward way. Such effects are very important in view of the essential role of actin for cell locomotion and cellular shape changes (Sackmann, 1994; Janmey et al., 1991). Another point is that in classical measurements of the frequency dependence of the viscoelastic moduli, the upper frequency limit is determined by the high mass or, for the torsional rheometer, the high moment of inertia of the experimental set-up. To overcome these problems, we built a magnetic bead micro-rheometer which allows local measurements of the time or frequency dependence of the viscoelastic moduli.

Magnetic bead techniques (using ferromagnetic beads) have been applied previously for studies of the viscoelasticity of the cell cytoplasm (Heilbronn, 1922; Crick and Hughes, 1950; Yagi, 1961; Sato et al., 1984) and F-actin networks (Zaner and Valberg, 1989) and for measurements of the viscoelastic properties of the vitreous body of the eye (Lee et al., 1993). Most of these studies were concerned with creep-response measurements, with the exception of the experiments by Lutz et al., who applied the oscillatory technique to measure the viscoelastic moduli of mucus using ferromagnetic beads of about 100 µm in diameter (Lutz et al., 1973). More recently, magnetic bead techniques have also been applied for the measurement of the bending stiffness of DNA filaments (Smith et al., 1992) and the cytoskeletal stiffness of cells (Wang et al., 1993). To our knowledge this is, however, the first attempt for quantitative measurements of the local viscoelastic parameters $G'(\omega)$ and $G''(\omega)$ of actin networks.

The micro-rheometer is based on the evaluation of the magnetically driven local motion of paramagnetic beads embedded in the networks by fast image processing techniques. Because of the low mass of the beads, our set-up allows much higher oscillation frequencies than the classical rheological

methods. The magnetic bead micro-rheometer offers three modes of operation: 1) recordings of the creep response and relaxation functions of the magnetic beads following pulse-like excitations; 2) measurements of the amplitudes and phase shifts of the motion of the beads excited by external oscillating magnetic fields which enable absolute measurements of the frequency dependence of the storage and loss moduli in the range 10^{-1} to 5 Hz; 3) evaluation of the trajectories of the beads through diluted networks under a constant force which yields simultaneously average values and spatial fluctuations of the viscosity.

The main purpose of the present work is to demonstrate that the magnetic bead micro-rheometer allows quantitative measurements of the absolute values of the two viscoelastic moduli.

MATERIALS AND METHODS

All measurements were performed in F-actin solutions of various concentrations. Globular actin (G-actin) and polymerization buffer (F-buffer) were prepared as previously described (cf. Ruddies et al., 1993).

The magnetic beads (Dynabeads, Dynal, Hamburg, Germany) used here are spherical latex particles (radius $a = 2.8$ μm $\pm$ 3%) with incorporated iron oxides. The uncertainty of the iron content is about 5–10% (Door et al., 1991). Since the incorporated iron oxide particles are smaller than Weiss domains, the beads exhibit paramagnetic behavior.

For preparation of our samples, the concentration of G-actin was first adjusted with millipore water. Subsequently, the beads and F-buffer were added. This solution was drawn into the sample cuvette by capillary forces and polymerized for about 6 h.

Fig. 1 a shows a schematic view of the rheometer mounted on a Zeiss inverted Axiomat microscope. The sample is contained in an elongated cuvette with rectangular cross-section (cf. Fig. 1 b). The oscillating magnetic driving field, $\tilde{B}(t)$, applied horizontally (perpendicular to the long axis of the cuvette). It is generated by two axisymmetrically arranged magnetic coils with cylindrical soft iron cores.

The force on the paramagnetic beads is

$$f(t) = M(t) \cdot \frac{dB(t)}{dx} = \chi \cdot B(t) \frac{dB(t)}{dx} \propto B(t)^2 \qquad (1)$$

where $M(t)$ is the induced magnetic moment of the bead. Since $f(t)$ is proportional to $B(t)^2$, we ran the programmable function generator with a $(\sin \omega t)^{1/2}$ waveform to obtain a sinusoidal force. The oscillatory motion of the beads is analyzed for a long time (compared to the reciprocal frequency) using a fast image processing system developed in this laboratory (Zilker et al., 1992; Peterson et al., 1992). It runs on a Maxvideo system (Datacube, Boston, MA) with the real-time operating system OS9–68k (Microware, Des Moines, IA).

The relative position of the bead and thus the amplitude of its oscillatory motion is measured by rapid on-line recording of the light intensity at video rate (25 Hz) along a bar of ~10 μm length aligned parallel to the axis of movement of the bead (cf. Fig. 1 c, left). Each of these intensity profiles is then fit by a Gaussian shape, the center of which is taken as the relative position of the center of mass of the bead. Thus, the accuracy of the determination of the bead position is much higher than the microscope resolution (~0.5 μm) and has been estimated to $\delta x \approx \pm 25$ nm at typical oscillation amplitudes of 1–2 μm. A typical displacement-time-graph is shown in Fig. 1 c (right).

The mutual phase shift of the beads with respect to the magnetic field is measured using an optical shutter which, at the end of each measurement, blocks the light beam exactly at phase $\varphi = 0$ of the signal. The accuracy $\delta\varphi$ of the phase measurement is thus limited by the video frequency of the image processing system (25 Hz) and the frequency ν of the oscillating magnetic field: $\delta\varphi = \pm \pi\nu/25$ Hz. The maximum dynamic range of the technique is about 0.01 Hz $\leq \nu \leq$ 50 Hz.
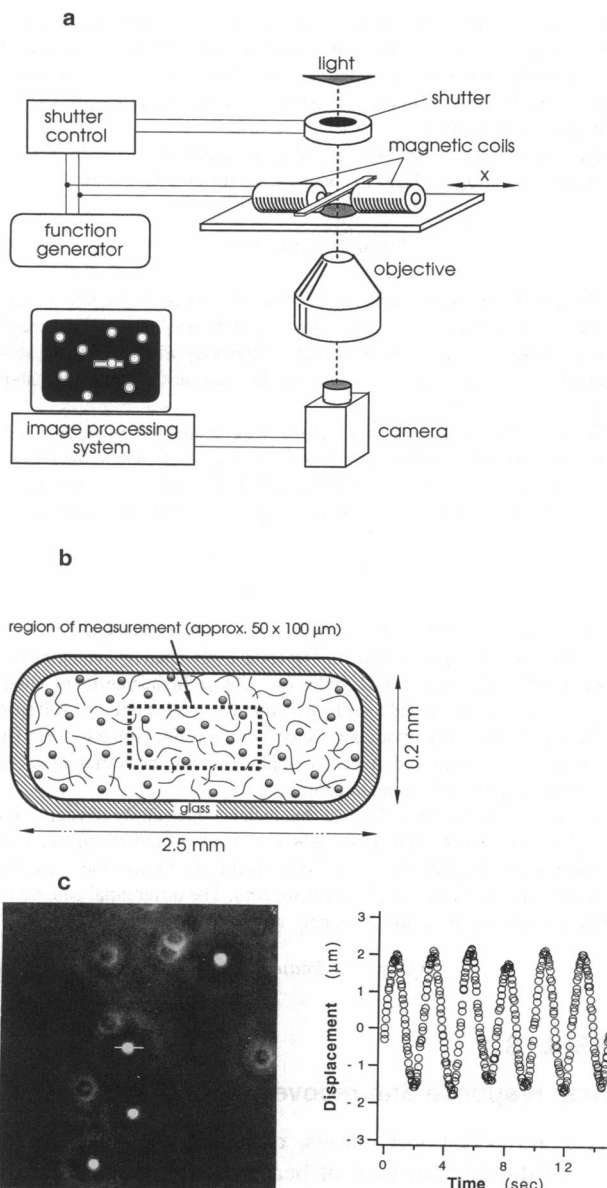

FIGURE 1 (a) Schematic view of micro-rheometer mounted on an inverted Zeiss-Axiomat microscope. The sample is contained in a rectangular cuvette (inner height 0.2 mm, inner width 2.5 mm). The magnetic field is produced by a pair of coils (length 15 mm, diameter 10 mm) into which cylindrical soft iron cores (diameter 5 mm) are inserted. The gap distance is 2.5 mm. A function generator drives both the magnetic field and the optical shutter. The oscillatory motion of the Dynabeads is analyzed by a fast image processing system. To determine the phase shift between force and response the initial position of the bead is determined after the end of each measurement using the optical shutter control. (b) Schematic illustration of a cross-section through the glass sample cell, showing the dimensions of the region where the viscoelastic measurements are performed. Note that the scale is compressed in the horizontal direction. (c) Left: Phase contrast image of beads embedded in actin network (not visible). The bar (~10 μm) indicates the area in which one-dimensional motion of the bead is analyzed. Right: Oscillatory motion of bead at excitation frequency $\omega/2\pi = 0.4$ Hz, showing the quality of the motion analysis.

To obtain absolute values of the viscoelastic moduli $G'(\omega)$ and $G''(\omega)$, the absolute force f_0 acting on the bead as well as the strain field around the bead must be determined.

The driving force f_0 can be calibrated with a bead in a pure viscous fluid of known viscosity (η) using constant or oscillating forces and applying

Stokes' law $f_0 = 6\pi a\eta\dot{x}$ (where a is the bead radius). To prevent sedimentation, we used glycerol-$CaCl_2$-water solutions with the density adjusted to $\rho \approx 1.3$ g/cm^3, approximately the density of the beads. For the set-up of magnetic coils used, an average maximum driving force of $f_0 \approx (0.53 \pm 0.10)$ pN was measured.

We now consider a bead embedded in a viscoelastic body. In this case the displacement of the bead is given by the differential equation

$$6\pi a\eta \frac{dx}{dt} + g\mu x = f(t) \qquad (2)$$

(neglecting the inertia of the bead). Here the first term on the left accounts for the viscous force as given approximately by Stokes' law, and the second term describes the elastic restoring force of the body with μ being the shear modulus and g a geometric constant that depends on the strain field about the sphere.

To obtain the elastic geometry factor g, we consider the principle of local perturbation (Love, 1944) assuming that the strain field due to the beads is equivalent to that of a point force. For a bead (of radius a) acting on the surface of a body, the strain field in the direction of the force (x) is

$$\delta x(\vartheta) = f_0 \frac{(1 + \cos^2\vartheta)}{4\pi a\mu} \qquad (3)$$

where ϑ is the angle between the direction of the force and the radius vector drawn from the origin of the sphere. The force is obtained by averaging over all angles in the half space which yields $\delta x = 3\pi a\mu$. In the interior of a body, the displacement is expected to be by a factor of 2 smaller since the full space has to be deformed. The elastic geometry factor g is thus equal to $6\pi a$. This result can be rigorously derived by application of the variation theory (M. Peterson, personal communication).

Therefore, in contrast to classical rheometers which apply constant strain throughout the sample, the strain field in our microbead rheometer is inhomogeneous. However, for small displacements the form of the strain field is incorporated in the geometric prefactor $6\pi a$. The differential equation of the bead motion is thus approximately given by

$$6\pi a\eta \cdot \dot{x} + 6\pi a\mu \cdot x = f(t). \qquad (4)$$

RESULTS

Creep response and recovery experiment

Fig. 2 shows response curves, $x_d(t)$, and relaxation curves, $x_r(t)$, of the displacement of beads in concentrated F-actin solution caused by repeated application of transient force pulses. For pulses of different duration, the response curves coincide within experimental error. Subtraction of the different curves showed that the average difference between any two response curves is $\Delta x \approx 40$ nm, which is smaller than our measurement precision of 50 nm. This shows that the entangled network behaves as a linear viscoelastic body and does not exhibit plastic behavior due to the irreversible structural changes of the network surrounding the beads.

With Eq. 4, the time dependence of the bead deflection, $x_d(t)$, following a force step function of amplitude f_0 may be expressed as

$$x_d(t) = J(t) \cdot \frac{f_0}{6\pi a} \qquad (5)$$

where $J(t)$ is the time dependent creep compliance of the network (Ferry, 1980) which is approximately equal to the reciprocal shear modulus of the network ($J(t) \approx \mu(t)^{-1}$).

If the stress is applied long enough, the velocity of the bead approaches a limiting value and a steady-state flow is at-
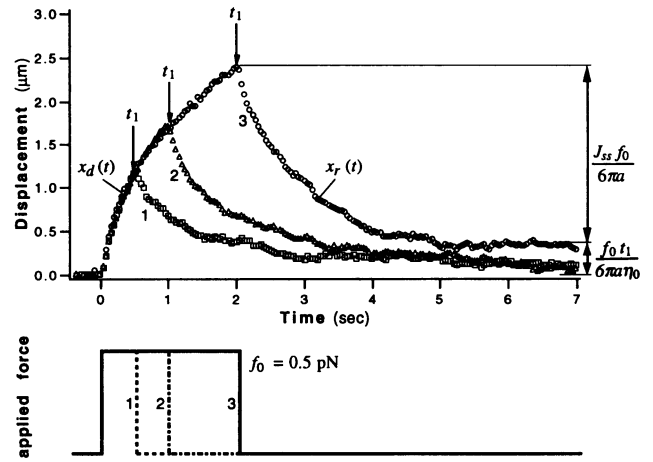

FIGURE 2   Creep response and relaxation function of beads in entangled F-actin solution (actin monomer concentration $c_A = 300$ μg/ml, mesh size $\xi \approx 0.6$ μm) (Schmidt et al., 1989) after application of 0.5 pN force pulses of various duration. Note that after the largest pulse width the bead relaxes to a new position.

tained. For this case, the creep response curve is dominated by the apparent viscosity of the network, η_0, giving

$$x_d(t) = \left\{ J_{ss} + \frac{t}{\eta_0} \right\} \cdot \frac{f_0}{6\pi a} \qquad (6)$$

where J_{ss} is the steady-state compliance. $J_{ss} \cdot f_0/6\pi a$ is a measure of the local elastic deformation of the network during steady flow (cf. Fig. 2).

The sudden removal of the force at $t = t_1$ can be interpreted as applying a second force $-f_0$. Following the Boltzmann superposition principle that effects of mechanical history are linearly additive, the creep relaxation function after the cessation of the force pulse at $t = t_1$ is

$$x_r(t) = \{J(t) - J(t - t_1)\} \frac{f_0}{6\pi a}. \qquad (7)$$

If steady flow is reached before cessation of stress, the creep relaxation function becomes

$$x_r(t) = \left\{ J_{ss} + \frac{t}{\eta_0} - J(t - t_1) \right\} \frac{f_0}{6\pi a} \qquad (8)$$

and approaches a final value $f_0 \cdot t_1/\eta_0$ (Ferry, 1980). This kind of creep recovery is represented by the displacement-time graph in Fig. 2, which corresponds to the longest duration of the force pulse ($t_1 = 2$ s).

In principle, J_{ss} can be obtained from the difference between the maximum displacement at $t = t_1$ and the limiting displacement $x_r(\infty)$ of the creep recovery:

$$J_{ss} = [x(t_1) - x(\infty)] \cdot 6\pi a/f_0.$$

The apparent viscosity of the network, η_0, is calculated from $6\pi a \cdot \eta_0 = f_0 \cdot t_1/x_r(\infty)$ (cf. Fig. 2). However, since the terminal relaxation times of entangled actin solutions are very long (10^4 s; Ruddies et al., 1993) such an analysis yields good estimates but not exact values of J_{ss} and η_0. For the experiment

shown here we calculated $J_{ss} \approx 108$ Pa^{-1} and $\eta_0 = 0.11$ Pa·s, consistent with our frequency dependent measurements mentioned below.

Frequency dependence of the viscoelastic moduli

For precise measurement of the viscoelastic behavior it is useful to apply an oscillating force $f(t) = f_0 \cdot \exp(i\omega t)$ on the beads. The frequency dependence of the storage modulus $G'(\omega)$ and the loss modulus $G''(\omega)$ are obtained by analyzing the amplitude $x_0(\omega)$ and the phase shift $\varphi(\omega)$ of the oscillatory motion of the excited beads. A typical response curve is shown in Fig. 1 c. The beads follow the dynamic equation (4) which is easily solved in the usual way by the ansatz $x(t) = x_0 \exp[i(\omega t - \varphi)]$ yielding the viscoelastic parameters

$$G'(\omega) = \frac{f_0}{6\pi a |x_0(\omega)|} \cdot \cos\varphi(\omega);$$

$$G''(\omega) = \frac{f_0}{6\pi a |x_0(\omega)|} \cdot \sin\varphi(\omega). \qquad (9)$$

These equations were also used by Lutz et al. (cf. Y. C. Fung, 1981). Fig. 3 shows plots of the frequency dependence of the storage modulus $G'(\omega)$ and the loss modulus $G''(\omega)$ of entangled actin networks of various concentrations. In all cases one observes a pronounced frequency dependence of G' and G''. For the two lowest concentrations (75 μg/ml and 100 μg/ml) both G' and G'' scale approximately as $\omega^{1/2}$. For the 300 μg/ml sample the $G'(\omega)$-vs-ω plot appears to exhibit a transition to a plateau at frequencies $\omega < 3$ rad/s while in the $G''(\omega)$-vs-ω plot the slope becomes larger for $\omega < 3$ rad/s.

The observed frequency dependencies of G' and G'' compare well with the results obtained by rotating disc rheology (Ruddies et al., 1993), where the low frequency regime (10^{-4} Hz $\leq \omega/2\pi \leq 1$ Hz) was studied. They found a plateau for $\omega/2\pi \leq 10^{-2}$ Hz and a frequency dependent regime for 10^{-2} Hz $\leq \omega/2\pi \leq 1$ Hz, in which $G'(\omega)$ and $G''(\omega)$ scale with the square root of the frequency. The present study thus shows that this law also holds for higher frequencies (up to 10 Hz). As shown previously (Ruddies et al., 1993), the plateau regime of $G'(\omega)$ can be explained in terms of the reptation dynamics of the polymer chains, while the frequency dependence is determined by the internal chain dynamics. The square root law is predicted for entangled solutions of polymers exhibiting Rouse dynamics.

The appearance of a plateau in $G'(\omega)$ and of an increase of the slope of $G''(\omega)$ at higher concentrations can be explained by assuming that the Rouse relaxation time τ_R decreases with decreasing mesh size. Indeed, the onset of the frequency dependent regime is determined by the reciprocal Rouse relaxation time (cf. Doi and Edwards, 1986). The longest wavelength excitation of the actin filaments is limited by the mesh size ξ and the Rouse relaxation time is thus expected to decrease with the square of the wavelength.

The absolute values we obtained for G' and G'' agree reasonably well with the values obtained previously (Müller et al., 1991). Deviations from those values by a factor of 2–3 can be explained by inhomogenities of the network, since the rotating disc rheometer averages over a large volume whereas with the present technique, it is possible to perform local measurements.

Continuous permeation mode

A continuous permeation experiment is shown in Fig. 4. It shows diagrams of distance versus time for beads in an entangled F-actin network with mesh size of the same order of magnitude as the bead diameter ($c_A = 75$ μg/ml, mesh size $\xi \approx 1.4$ μm). For comparison, in Fig. 4 b we also show the x-t diagram of a bead in a glycerol-CaCl$_2$-solution (25 wt % of glycerol, viscosity: $\eta = 31.4$ mPa·s). Clearly, the local velocity of the bead $\vec{v}_{loc} = dx/dt$ fluctuates much more in the F-actin solution than in the normal fluid, demonstrating the local graininess of the polymeric liquid. Most of the time the bead moves with a constant average velocity of $\bar{v} = 0.65$ μm/s. However, fluctuations occur on two time and/or length scales:

(1)   At a few sites, the velocity is slowed down or increased remarkably (typically by a factor of 2) over time scales of about 5 s (cf. regions indicated by thick arrows in Fig. 4 a).

(2)   In the regime in which the bead moves with the average velocity $\bar{v}$, the x-t curve exhibits local fluctuations on time scales of less than 1 s and length scales of ≤ 1 μm as shown more clearly in the enlargements of Fig. 4 b. Occasionally stepwise motions of height on the order of the mesh size ($\xi \approx 1.4$ μm) are seen (cf. arrows in Fig. 4 b). Moreover, small displacements in the negative direction are observed.

The bead motion can be described in terms of a Langevin equation with a space dependent viscosity $\eta(x)$ and three types of fluctuating forces:

$$6\pi a \eta(x) \cdot \dot{x} = f_0 + f^s_B + f^s_{e1} + f^s_{e2}, \qquad (10)$$

where f^s_B is the random force due to thermal fluctuations of the solvent and is approximately equal to the fluctuating forces in pure solvents.

f^s_{e1} accounts for the fluctuating elastic force due to spatial fluctuations of the mesh size resulting in corresponding fluctuations of the creep compliance. These forces are responsible for the slow fluctuations of the velocity.

f^s_{e2} is the random elastic force exerted by the bending fluctuations of the filaments. These are assumed to be responsible for the short time fluctuations of the beads and their occasional displacement in the negative x direction.

The two elastic contributions to the random force determine the width of the velocity distribution shown in Fig. 4 c. From the average slope of the x-t diagram of Fig. 4 a one obtains a mean velocity from which an average value of the apparent viscosity of the entangled solution can be calculated according to $\bar{\eta}$. From this value one estimates an elastic loss modulus for very low frequencies: $G''(\omega \approx 0) = 0.002$ J/m^3. This agrees well with the value of the loss modulus obtained from the analysis of the oscillatory motion at the lowest frequency ($G''(0.1$ Hz, $c_A = 75$ μg/ml) ≈ 0.004 J/m^3).
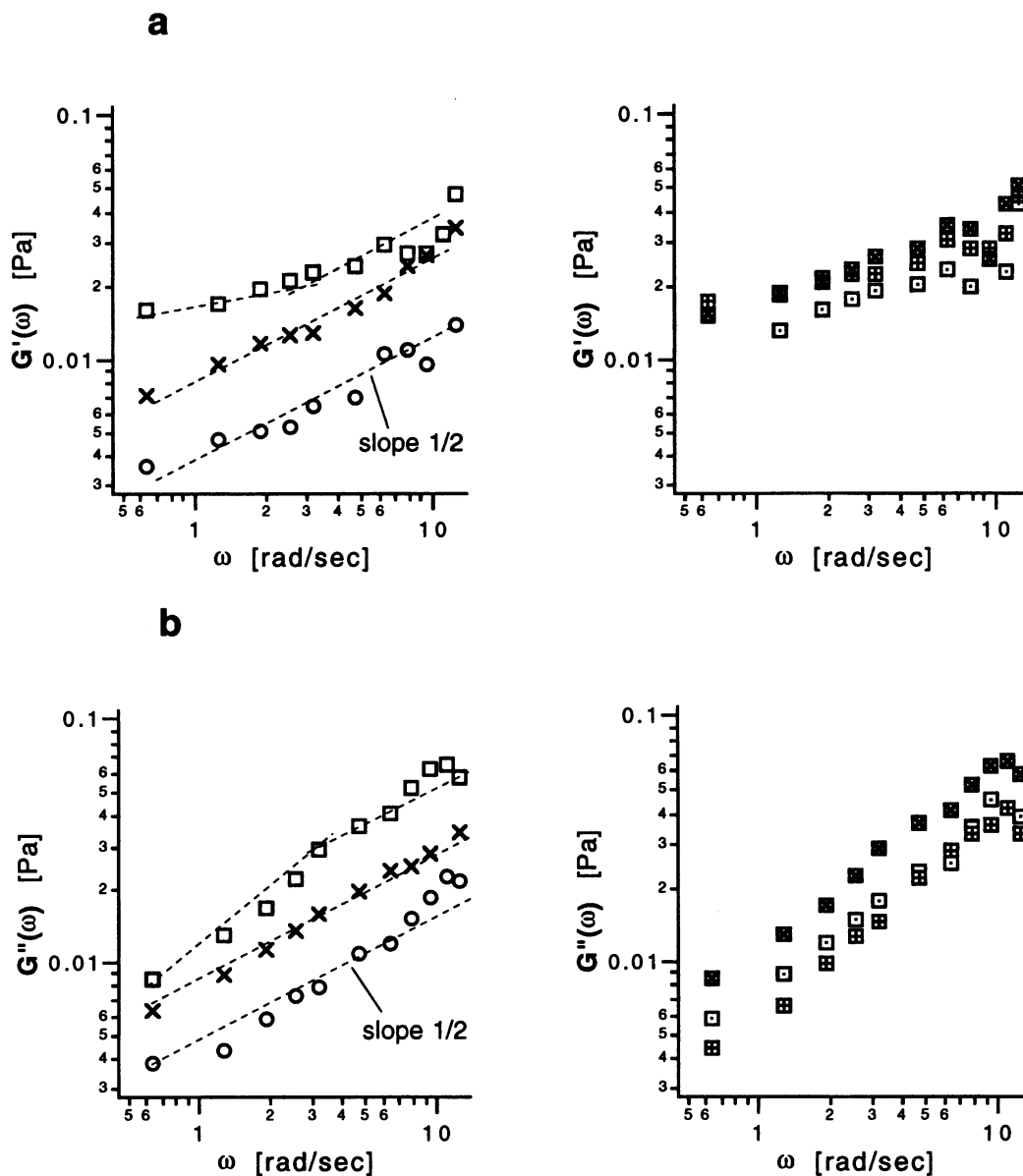
FIGURE 3   (a) *Left:* Frequency dependence of storage modulus for entangled F-actin solutions for three different actin monomer concentrations: 75 μg/ml (○), 100 μg/ml (×) and 300 μg/ml (□). The corresponding mesh sizes ξ are 1.4 μm, 1.0 μm, and 0.6 μm. Note that the data points for the two lowest actin concentrations lie reasonably well on a straight line of slope 1/2. *Right:* Measurement of $G'(\omega)$ at three different positions within the entangled solution showing variance of local storage modulus. (b) *Left:* Frequency dependence of loss modulus for the same solutions. The data for the two lowest concentrations again obey a scaling law $G''(\omega) \propto \omega^{1/2}$. *Right:* Measurement of $G''(\omega)$ at three different positions within the entangled solution showing variance of local loss modulus.

From the slow variations of the slope dx/dt, the fluctuations of the loss modulus can be estimated. Analysis of the x-t diagram in Fig. 4 a yields $\delta G'' \approx \pm 0.002 \, J/m^3$. Note that the total width of the velocity distribution in Fig. 4 c is also determined by the force due to the chain bending excitations. More detailed work on the local fluctuations is currently in progress.

DISCUSSION

The main purpose of the present work was to demonstrate that microrheology based on the oscillating magnetic bead method allows quantitative, local measurements of the frequency dependence of the viscoelastic moduli in entangled F-actin solutions. The technique is particularly well suited for rheological studies of dilute networks of biological polymer filaments which are very soft and exhibit mesh sizes on the micrometer scale. By using larger magnetic fields (and correspondingly smaller beads), the method can easily be extended to networks with smaller mesh sizes. Since the beads can be moved within the gels, the micro-rheometer allows sequential measurements at different sites to probe large scale fluctuations of soft and heterogeneous biogels. As demonstrated in the present work, small scale fluctuations of
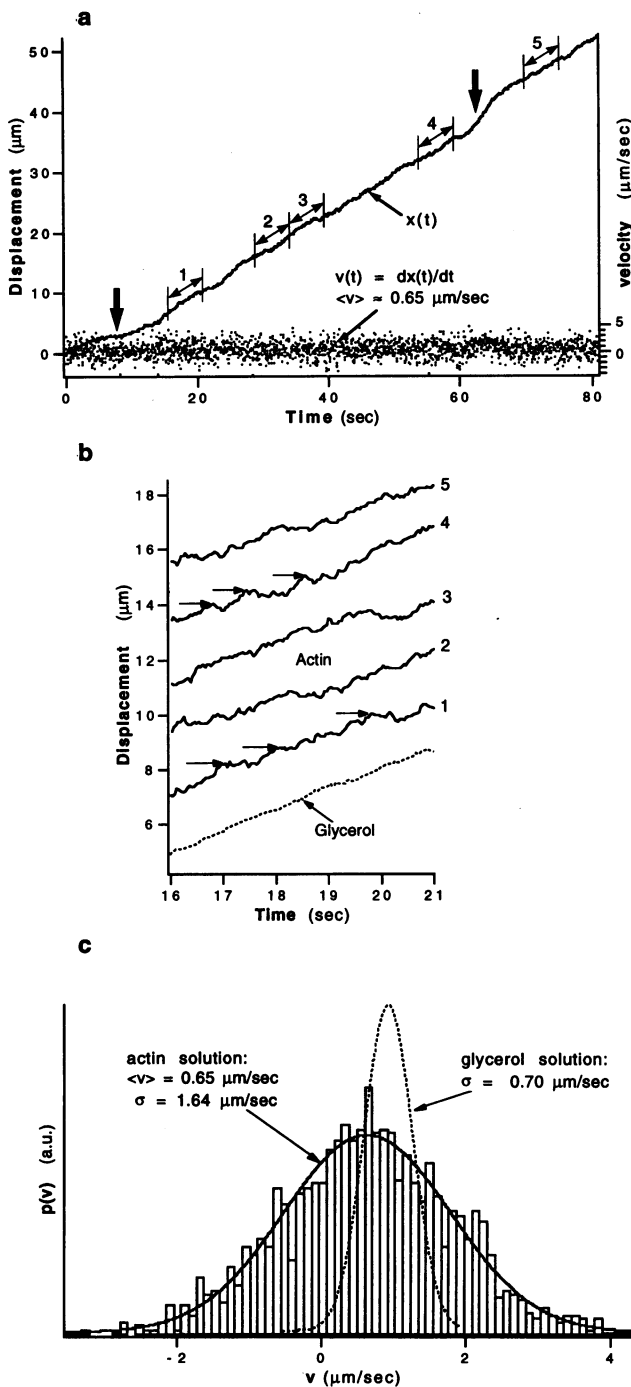
homogeneous networks can be evaluated most conveniently by observing fluctuations in the local velocity $\vec{v}_{loc}$ of a selected bead.

The present instrument yields reliable quantitative values of the viscoelastic moduli $G'(\omega)$ and $G''(\omega)$ in the frequency regime between 0.1 and 10 Hz. It thus extends the dynamic range of a previously designed magnetically driven rotating disc rheometer (Müller et al., 1991) to higher frequencies. An extension to even higher frequencies would be possible using an improved image processing system. The present method can therefore bridge the gap between dynamic light scattering and conventional rheological measuring techniques.

The application of micro beads as force transducers in cell biology is an active field of research. Although the force on magnetic beads generated in our set-up is still very low ($\approx$pN), in situ measurements of the viscoelasticity within cells should be possible. In contrast to optical tweezers, magnetic beads cannot be as easily maneuvered. However, quantitative measurements as shown in this article are more easily obtained.

REFERENCES

Crick, F. H. C., and A. F. W. Hughes. 1950. The physical properties of cytoplasm. A study by means of magnetic particle method part I. Experimental. *Exp. Cell Res.* 1:37–80.

Doi, M., and S. F. Edwards. 1986. The Theory of Polymer Dynamics. Clarendon Press, Oxford. 228.

Door, R., D. Frösch, and R. Martin. 1991. Estimation of section thickness and quantification of iron standards with EELS. *J. Microsc.* 162:15–22.

Ferry, J. D. 1980. Viscoelastic Properties of Polymers. John Wiley & Sons, New York. 10, 17–20.

Fung, Y. C. 1981. Biomechanics. Springer-Verlag, New York. 177–180.

Heilbronn, A. 1922. Eine neue Methode zur Bestimmung der Viskosität lebender Protoplasten. *Jahrb. Wiss. Bot.* 61:284–338.

Janmey, P. A. 1991. Mechanical properties of cytoskeletal polymers. *Curr. Opin. Cell Biol.* 3:4–11.

Janmey, P. A., S. Hvidt, J. Lamb, and T. P. Stossel. 1990. Resemblance of actin-binding protein/actin gels to covalently crosslinked networks. *Nature.* 345:89–92.

Käs, J., H. Strey, and E. Sackmann. 1993. Direct measurement of the wave-vector-dependent bending stiffness of freely flickering actin filaments. *Europhys. Lett.* 21:865–870.

Kerst, A., C. Shmielewsky, C. Livesay, R. E. Buxbaum, and S. R. Heidemann. 1990. Liquid crystal domains and thixotropy of filamentous actin suspensions. *Proc. Natl. Acad. Sci. USA.* 87:4241–4245.

Lee, B., M. Litt, and G. Buchsbaum. 1993. Rheology of the vitreous body. I: Viscoelasticity of the human vitreous. *Biorheology.* 29:521–534.

Love, A. E. H. 1944. A Treatise on the Mathematical Theory of Elasticity. Dover Publications, New York. 189–192.

Lutz, R. J., M. Litt, and L. W. Chakrin. 1973. Physical-chemical factors in mucus rheology. *In* Rheology of Biological Systems. H. L. Gabelnick and M. Litt, editors. Charles C Thomas, Springfield, IL. 119–157.

Müller, O., H. E. Gaub, M. Bärmann, and E. Sackmann. 1991. Viscoelastic moduli of sterically and chemically cross-linked actin networks in the dilute to semi-dilute regime: measurements by an oscillating disk rheometer. *Macromolecules.* 24:3111–3120.

FIGURE 4   (*a*) *Solid curve:* Displacement versus time diagram of bead drawn through the network (actin concentration $c_A = 75$ μg/ml corresponding to a mesh size $\xi = 1.4$ μm) at constant force ($f_0 \approx 0.35$ pN). *Dotted curve:* Velocity versus time diagram showing an average velocity of $\langle v(t) \rangle = \langle dx(t)/dt \rangle \approx 0.65$ μm/s. *Thick arrows:* Regions where the bead velocity differs remarkably from $\langle v \rangle$. (*b*) Enlargement of displacement versus time diagrams taken at the positions indicated by double arrows along the *x-t* curve in Fig. 4 *a*. The small arrows indicate stepwise motions of the bead. The dashed line shows an *x-t* diagram of the bead in aqueous glycerol solution of viscosity $\eta = 31.4$ mPa·s. (*c*) Histogram of the local velocity of a bead, $v_{loc} = dx/dt$, obtained from the distribution of the local slope of *x-t* curve shown in Fig. 4 *a*. *Solid curve:* Gaussian fit to velocity distribution of bead in actin solution. *Dashed curve:* Gaussian fit to velocity distribution of bead in glycerol solution.

Peterson, M., H. Strey, and E. Sackmann. 1992. Theoretical and phase contrast microscopic eigenmode analysis of erythrocyte flicker: amplitudes. *J. Phys. II France.* 2:1273–1285.

Ruddies, R., W.H. Goldmann, G. Isenberg, and E. Sackmann. 1993. The viscoelasticity of entangled actin networks: the influence of defects and modulation by talin and vinculin. *Eur. Biophys. J.* 22:309–321.

Sackmann, E. 1994. Intra- and extracellular macromolecular networks: physics and biological function. *Macromol. Chem. Phys.* 195:7–28.

Sato, M., T. Z. Wong, D. T. Brown, and R. D. Allen. 1984. Rheological properties of living cytoplasm: a preliminary investigation of squid axoplasm (*Loligo pealei*). *Cell Motil.* 4:7–23.

Smith, S. B., L. Finzi, and C. Bustamante. 1992. Direct mechanical mea-

surements of the elasticity of single DNA molecules by using magnetic beads. *Science.* 258:1122–1126.

Wang, N., J. P. Butler, and D. E. Ingber. 1993. Mechanotransduction across the cell surface and through the cytoskeleton. *Science.* 260:1124–1127.

Yagi, K. 1961. The mechanical and colloidal properties of *Amoeba* protoplasm and their relations to the mechanism of amoeboid movement. *Comp. Biochem. Physiol.* 3:73–91.

Zaner, K. S., and P. A. Valberg. 1989. Viscoelasticity of F-actin measured with magnetic microparticles. *J. Cell Biol.* 109:2233–2243.

Zilker, A., M. Ziegler, and E. Sackmann. 1992. Spectral analysis of erythrocyte flickering in the 0.3–4 μm^{-1} regime by microinterferometry combined with fast image processing. *Phys. Rev. A.* 46:7998–8001.